Temperature Rise Effect of Permanent Magnet Wind Turbine in Different Field Settings

SHUYE DING, MIN ZHU, YING WANG, AND WEI LIU
Electrical Engineering and Automation, Nanjing Normal University, Nanjing, China

Corresponding author: Shuye Ding (dingshuye@163.com)

ABSTRACT Temperature rise is an essential factor affecting the safety operation of electric machines. An appropriate solving domain is the first step to consider when calculating the temperature rise. However, the effect of solving domain setting on the calculation results of electric machine temperature rise has not been deeply discussed. In this paper, a 3MW permanent magnet wind generator is taken as an example. Based on the electrical and numerical heat transfer theories, two different solving domain models are established to compare the flow thermal characteristics of the internal and external ventilated paths. The fluid velocity changes in external ventilated path, the central section temperature rise and the velocity trace distribution of the internal ventilated path are compared in detail. Furthermore, the temperature rise of each component is analyzed. It is found that the fluid development in the generator is affected by solving domain selection. The results can provide a reference for accurate calculation of temperature rise of permanent magnet wind generator.

INDEX TERMS Flow-thermal coupling, permanent magnet wind generator, solution region setting, temperature field.

I. INTRODUCTION

In recent years, wind energy has been widely used in various fields in order to alleviate the shortage of traditional energy. The European Wind Energy Association points out that the new installed capacity of wind power in the world will reach 1200GW by 2020. Permanent magnet wind generators is one of the most popular wind turbines due to its safety operation and high reliability [1]–[3]. However, with the increasing capacity of permanent magnet wind generator, the operation loss will increase significantly. As a consequence, the temperature rise inside the generator will also increase, and the safety of the generator will be affected. Therefore, it is necessary to study the temperature rise effect intensively when designing the generator.

In general, using cooling system is a straightforward way to reduce the temperature rise effect. According to different cooling media, the cooling systems can be divided into natural air cooling, forced air cooling and liquid cooling [4]–[9]. In a small power machine, natural air cooling system is usually used. If the power level of machine is high, forced air cooling will be adopted in order to strengthen the

The associate editor coordinating the review of this manuscript and approving it for publication was Huiqing Wen.

TABLE 1. The comparison of different cooling systems.

	Natural air cooling	Forced air cooling	Liquid cooling
Power level	<2~3MW	≤5MW	>5MW
Cost	Cheap	Middle	Expensive
Cooling effect	Poor	Middle	Good
Efficiency	High	Middle	Low
Reliability	High	Middle	Low

cooling effect. Unlike the natural air cooling and forced air cooling, the liquid cooling system uses water or oil rather than air to transfer heat to the air. The comparison of three cooling systems is shown in TABLE 1.

Optimization of cooling structure is another approach to achieve this aim. For instance, the thermal characteristics effect of potting of the stator in generator has been analyzed by Polikarpova et al. [10]. The thickness of the iron core lamination and the number of ducts has been changed by Liu et al. to study the temperature distribution of the motor [11]. The thermal behavior of windings is studied in [12]–[14], which validates that the effective improvements of integral-slot distributed winding and end windings by high-heat-conductance material. In addition, other components have also been research interests by some researchers, such

as rotor [15], windshield [16], ventilation spacer [17], stator clamping plate [18] and junction boxes [3].

Although temperature rise of electric machines can be reduced by the two aforementioned approaches, the selection of solving domain has been ignored and not been deeply studied in the previous research. Generally, partial solving domain will be selected to analyze by researchers in order to save the calculation time, such as 1/48 of the whole machine [4], 1/36 along the circumferential direction of the structure [5] and half an axial segment along the axial direction of the machine [19]. It should be noted that the different solving domain cause different simulation results. How to select a suitable domain has not been properly discussed yet.

In order to fill this gap, the effect of solving domain setting on the calculation results of electric machine temperature rise is studied in this paper. A 3MW permanent magnet wind generator is used as the research object. Combined the features of Table 1, forced air cooling is selected as cooling system in this paper. Based on the electrical and numerical heat transfer theories, two different solution region models are established to compare the fluid and thermal characteristics of the generator. The fluid velocity changes in external ventilated path are studied, and the temperature rise of each component is analyzed in detail. The results of the study will provide a theoretical basis for accurate calculation of permanent magnet wind generator.

II. MATHEMATICAL MODEL

The flow of fluid in a generator must follow the three conservation laws of mass, energy and momentum, When the fluid is incompressible and stable, the general form of the governing equation is as follows [20]:

$$div\,(\rho u\phi) = div\,(\Gamma\,grad\phi) + S \tag{1}$$

The expansion form as in (2):

$$\frac{\partial}{\partial t}(\rho\phi) + \frac{\partial}{\partial x}(\rho u\phi) + \frac{\partial}{\partial y}(\rho v\phi) + \frac{\partial}{\partial z}(\rho w\phi)$$
$$= \frac{\partial}{\partial x}\left(\tau\frac{\partial\phi}{\partial x}\right) + \frac{\partial}{\partial y}\left(\tau\frac{\partial\phi}{\partial y}\right) + \frac{\partial}{\partial z}\left(\tau\frac{\partial\phi}{\partial z}\right) + S \tag{2}$$

where ρ is the fluid density $\left(kg/m^3\right)$; ϕ is the general variable; S is the source term; Γ is the extension variable.

Based on the numerical heat transfer theory, considering the anisotropy of the medium, the three-dimensional heat conduction equations in the solution region are as follows [21]:

$$\left.\begin{array}{r}\dfrac{\partial}{\partial x}\left(\lambda_x\dfrac{\partial T}{\partial x}\right) + \dfrac{\partial}{\partial y}\left(\lambda_y\dfrac{\partial T}{\partial y}\right) + \dfrac{\partial}{\partial z}\left(\lambda_z\dfrac{\partial T}{\partial z}\right) \\ = -q_V \\[4pt] \left.\dfrac{\partial T}{\partial n}\right|_{S_1} = 0 \\[4pt] \left.-k\dfrac{\partial T}{\partial n}\right|_{S_2} = -\alpha\,(T - T_f)\end{array}\right\} \tag{3}$$

where $\lambda_x, \lambda_y, \lambda_z$ are thermal conductivity of different materials along x, y, z axes $(W/(m \cdot K))$; T is the temperature

to be solved (°C); q_V is the total heat source value in the generator $\left(W/m^3\right)$; S_1 is the adiabatic surface; S_2 is the heat dissipation surface; α is the heat dissipation coefficient $\left(W/\left(m^2 \cdot K\right)\right)$; T_f is the ambient temperature (°C).

III. ESTABLISHMENT OF PHYSICAL MODEL
A. BASIC ASSUMPTIONS
In order to facilitate calculation, the following assumptions are made according to the actual ventilation structure characteristics of the generator [21]:

1) This paper only discusses the steady state of the fluid, the governing equation does not contain time term.

2) Since the flow rate is much lower than the sound velocity, the fluid is regarded as incompressible.

3) The end strand of the stator is treated as a straight line segment.

4) All parts of the generator are evenly dipped and well insulated.

5) The cooling effect of the cooler on the circumference of the generator is the same.

B. PHYSICAL MODEL
The cross section of the generator is shown in Fig. 1. The generator selected in this paper has two ventilated path, the internal ventilated path is shown by the red arrow, and external ventilated path is shown by the blue arrow.
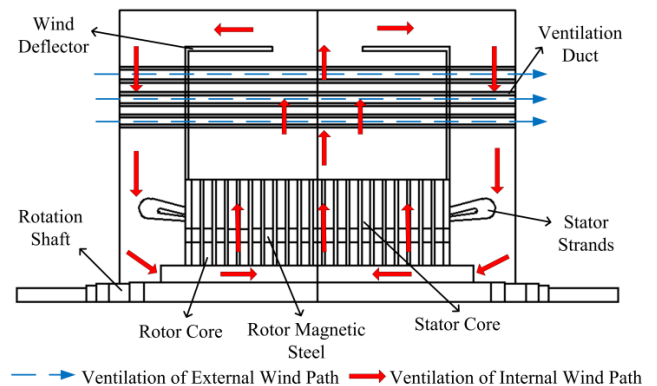

FIGURE 1. The cross section of generator.

The solution region cannot be selected too large because of the restrict of the computer ability, and the reasonable simplification of the model will not only have a great impact on the calculation results, but also save time for calculation and analysis obviously. According to the characteristics of symmetrical structure of permanent magnet wind generator, a complete slot, two half-teeth and half axial section of the generator are taken as the solution region in the first model, a complete slot, two half-teeth and the whole axial segment of the generator are taken as the solution region in the second model. The physical model of the solution region is shown in Fig. 2.

The primary cooling gas passes through the rotor axial duct, the rotor radial duct, the air gap, the stator radial duct,
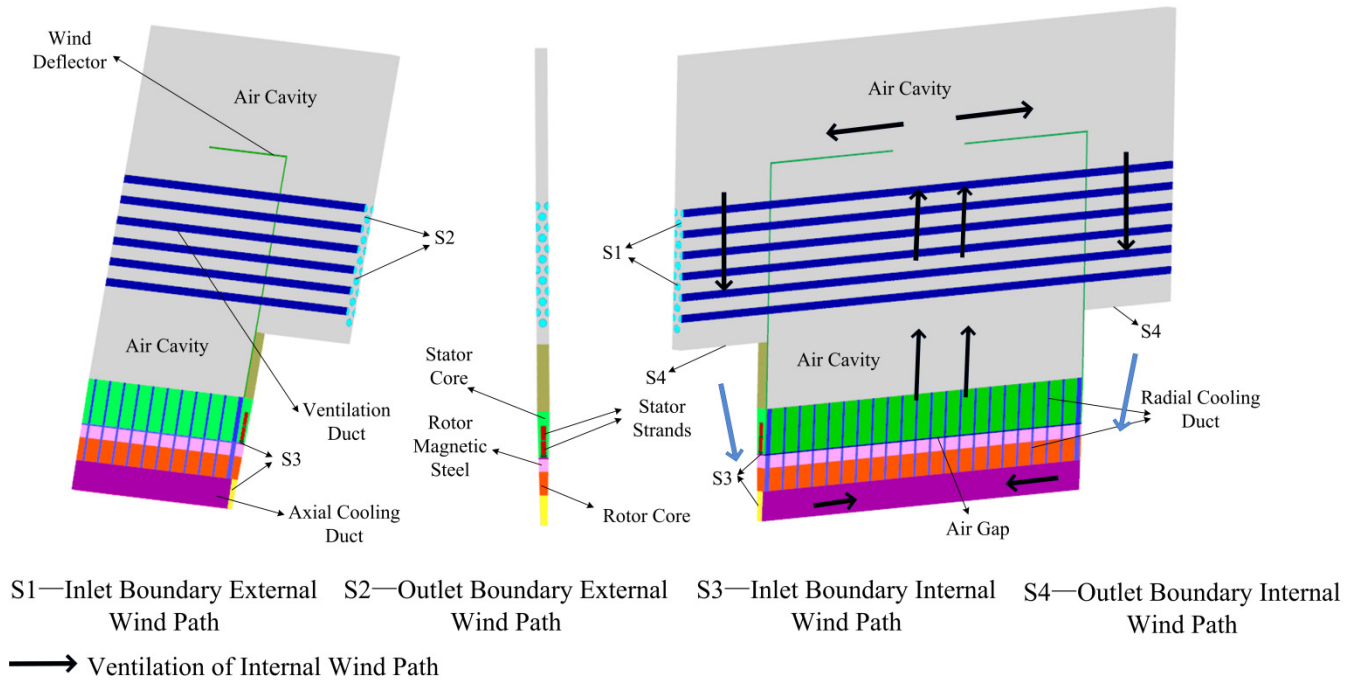
S1—Inlet Boundary External Wind Path   S2—Outlet Boundary External Wind Path   S3—Inlet Boundary Internal Wind Path   S4—Outlet Boundary Internal Wind Path

→ Ventilation of Internal Wind Path

FIGURE 2. Physical model of the solution region.

TABLE 2. The loss distribution of generator.

Loss (kW)	Stator Copper Loss	Stator Iron Loss	Rotor Iron Loss	Additional Loss
	32	23	1.3	16

the cooler and the air cavity in turn. The wind deflector is used to restrain the flow direction of the fluid. The cooling process of the external ventilated path is that the fan continuously pushes the secondary cooling gas into the cooling pipe, which flows through the cooling pipe at a high flow rate, and then exchanges heat with the primary cooling gas, which can take away heat.

Generator will produce a variety kinds of losses under rated operating conditions. The loss distribution of each part of a permanent magnet wind generator is obtained by electromagnetic calculation, as shown in TABLE 2.

C. BOUNDARY CONDITIONS

The specific boundary conditions of the solution region are as follows:

1) The velocity inlet is used as the entrance boundary condition. The velocity of the external ventilated path is 33.4 m/s, and the velocity of the internal ventilated path is 4.85 m/s.

2) The pressure outlet is used as the outlet boundary condition. The initial pressure is a standard atmospheric pressure.

3) The ambient temperature of the external wind path in half of the axial section is set as 310k, and in the whole axial section is 300k.

4) The boundary surface of the solution region and the axial central section of the whole axial section are set as adiabatic surfaces.
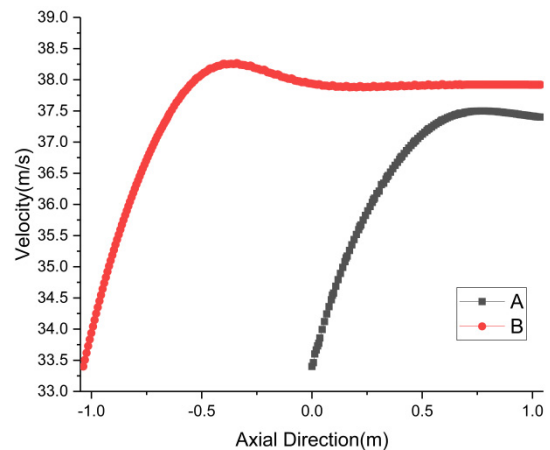

FIGURE 3. The axial wind velocity of the external wind path.

IV. ANALYSIS OF EXTERNAL VENTILATED PATH CALCULATION

The left model in Fig.2 is set as scheme A, and the right model is set as scheme B. In order to observe the influence of field selection on external ventilated path, the axial ventilated velocity of the ventilation duct in the center of the external ventilated path is measured. The graph is shown in Fig. 3.

According to Fig. 3, the inlet velocity of scheme A and scheme B are both 33.4 m/s. The initial cooling medium flow rate increases monotonically because of the narrow pipe, and then the flow rate decreases slightly and finally becomes stable due to the existence of friction resistance between the fluid and the pipe wall. Obviously, although the distribution

trend of the two schemes is similar, the velocity of scheme A is significantly lower than that of scheme B, the maximum velocity differs by 0.78 m/s. The length of circulation path of scheme A is only 1/2 of scheme B, so the fluid is not fully developed and the velocity of the fluid does not reach a steady state when it reaches the outlet, which affects the calculation results to a certain extent.

Section 2.3 shows that the inlet ambient temperature of scheme A is set as 310k, which is calculated according to empirical formula $CM\Delta T = Q$. In order to verify the rationality of solution region selection and boundary condition setting, the ventilation pipes at the center of the external wind path are numbered 1~6 from bottom to top. This paper takes the central section of scheme B (z = 0, namely the entrance boundary of scheme A) for analysis.
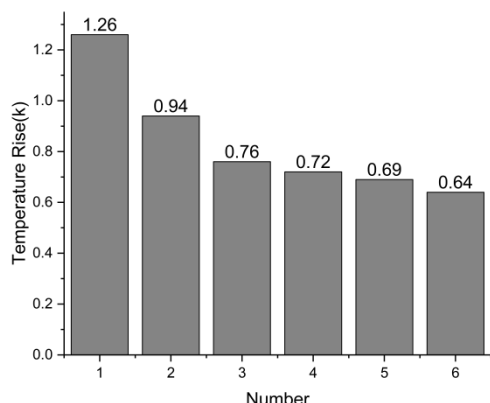

FIGURE 4. Section z = 0 temperature rise value of ventilation pipe.

Fig. 4 is the temperature rise column diagram of cross-section ventilation pipe. From Fig. 4, we can see that the maximum temperature rise is 1.26k and the average temperature rise is 0.835k. Due to the energy loss caused by wind resistance and friction in the ventilation pipe, scheme A produces errors, however, the error value is within the allowable range, indicating that the region selected in scheme A is reasonable. In addition, the temperature rise of the ventilation pipe decreases from bottom to top because the small number of the ventilation pipe is close to the heat source, and the heat transfer phenomenon is obvious.

V. ANALYSIS OF INTERNAL VENTILATED PATH CALCULATION

A. ANALYSIS OF FLUID FIELD

When the cooling gas is in a constant flow, that is, in a stable state, the streamline of the fluid coincides with the trace. Fig. 5 and Fig. 6 show the traces of cooling medium in the internal air circuit of the generator.

It is not difficult to see that the velocity of scheme B is slightly higher than that of scheme A. The fluid flows from the axial ventilation duct of the rotor to the radial ventilation duct of the stator and rotor and then flows into the air cavity. Because of the existence of stator windings and the flow area
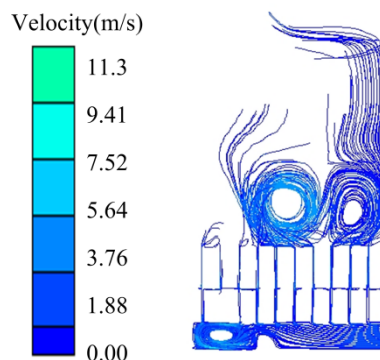

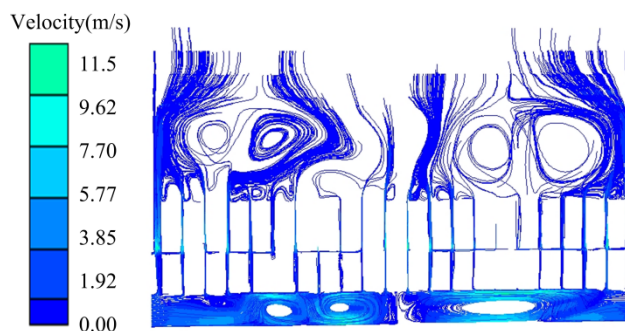**FIGURE 5.** Internal wind trace of scheme A.

FIGURE 6. Internal wind trace of scheme B.

becomes larger suddenly, vortex flow occurs at the end of the stator and in the air cavity. The vortex flow is also one of the reasons for the uneven heat dissipation and temperature rise in the generator.

Due to the complex law of fluid flow in the whole region, section z = −0.279m in the axial direction is taken to analyze the flow state of the cooling medium. The center line of the region is used to analyze the change of the flow velocity. Fig. 7 shows the velocity curve of the sampling line in two fields.

As can be seen from Fig. 7:

1) The wind speed in the ducts changes complex. The inlet wind speed contains large axial and circumferential components, and the fluid velocity in the rotor axial ventilation duct changes dramatically.

2) The area with a velocity of 0 at the left end is due to the stator copper wire blocking the flow of the cooling medium. In the area of y = 0.68m~0.98m, the highest flow rate is less than 2m/s. The reason why the overall flow velocity in this region is low is that the vortex flow exists at the end of the stator copper wire and the flow area becomes larger when the fluid enters the air cavity. In the area of y = 0.98m~1.818m, because of the existence of ventilation duct, the velocity curve fluctuates, and the large area of the air cavity leads to the low velocity.

3) In general, the average wind speed of scheme B is about 3.67m/s, which is 0.25m/s higher than that of scheme A.
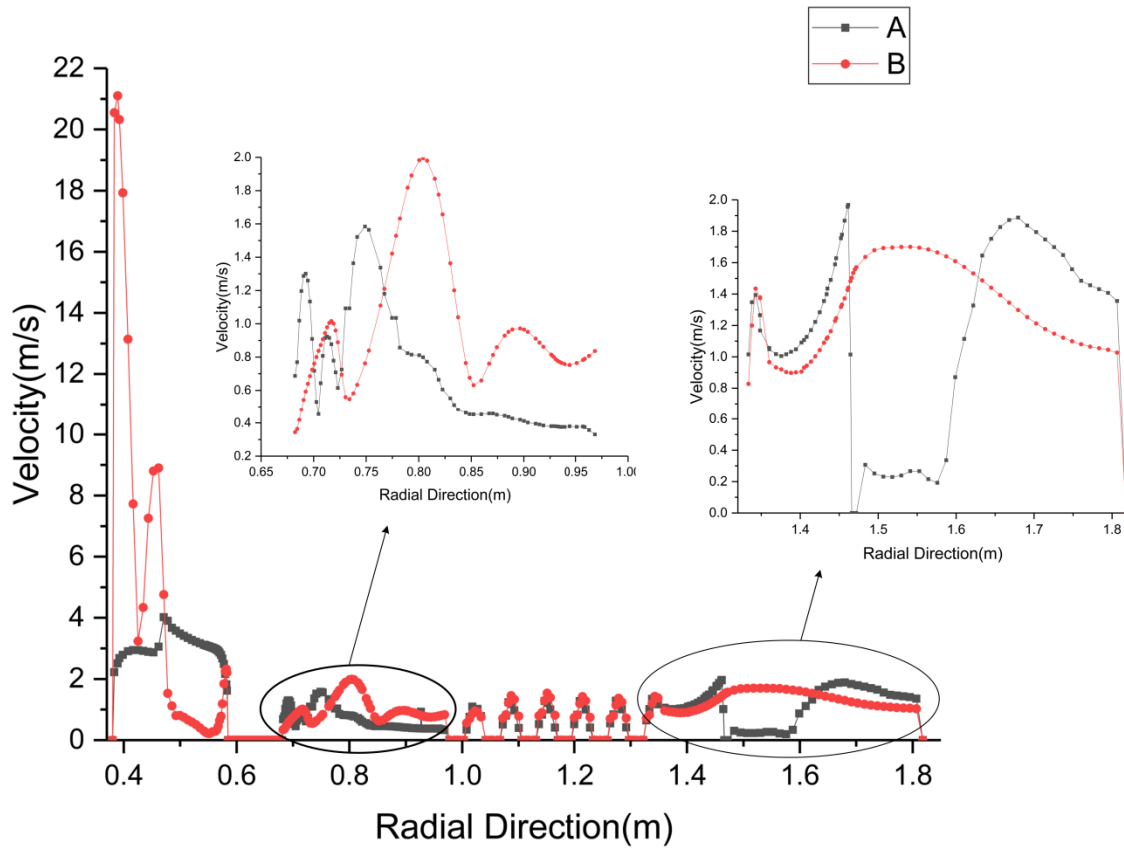
FIGURE 7. Section z = −0.279m center line velocity curve distribution.

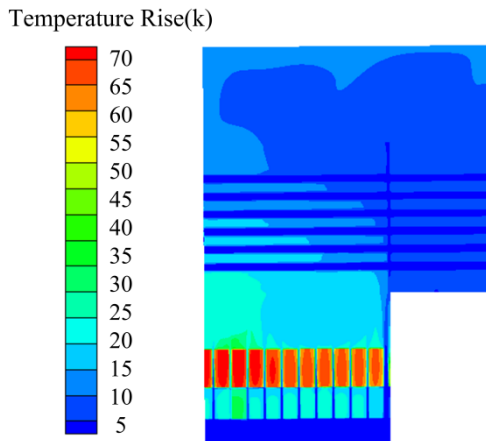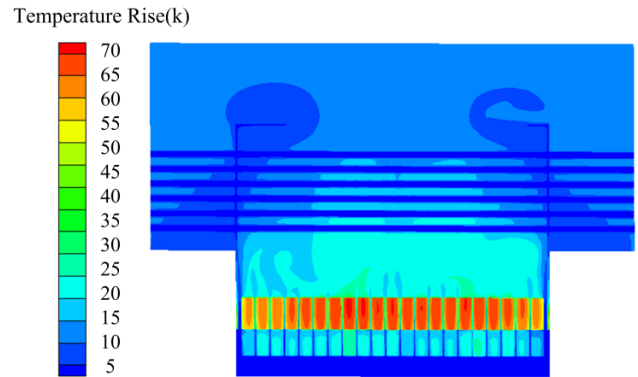**FIGURE 8.** Temperature rise distribution cloud map of scheme A.

FIGURE 9. Temperature rise distribution cloud map of scheme B.

B. ANALYSIS OF TEMPERATURE FIELD

In order to further explore the difference of temperature rise effect under different field settings, the temperature field of the ventilated path in the two schemes is calculated. Fig. 8 and Fig. 9 show the overall temperature rise cloud maps of the two schemes.

According to Fig. 9, the temperature rise distribution of the generator is roughly about axisymmetric, and the cooling medium accumulates at the windshield. The radial distribution tends to increase first and then decrease, this indicates that the cooling medium in the ventilation duct takes away the heat generated inside the generator well. Compared with Fig. 8, Fig. 9 shows that the temperature rise distribution tends to be consistent.

TABLE 3 and TABLE 4 give the maximum temperature rise and average temperature rise of components respectively.

From TABLE 3 and TABLE 4, it can be noticed that the maximum temperature rise of scheme A is 74.86k, while that

TABLE 3. Maximum temperature rise of each component.

	Upper Strands (k)	Lower Strands (k)	Rotor Core (k)	Stator Core (k)	Rotor Magnetic Steel (k)
Scheme A	72.42	74.46	32.13	74.86	31.31
Scheme B	73.78	75.95	29.01	76.87	28.51
Difference %	1.8	2	-9.7	2.7	-8.9

TABLE 4. Average temperature rise of each component.

	Upper Strands (k)	Lower Strands (k)	Rotor Core (k)	Stator Core (k)	Rotor Magnetic Steel (k)
Scheme A	69.5	70.96	21.99	67.15	20.24
Scheme B	71.29	73.34	20.75	70.26	19.39
Difference %	2.6	2.38	-5.6	4.6	-4.2
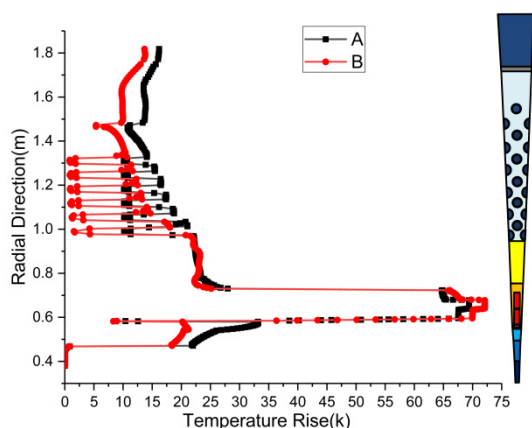
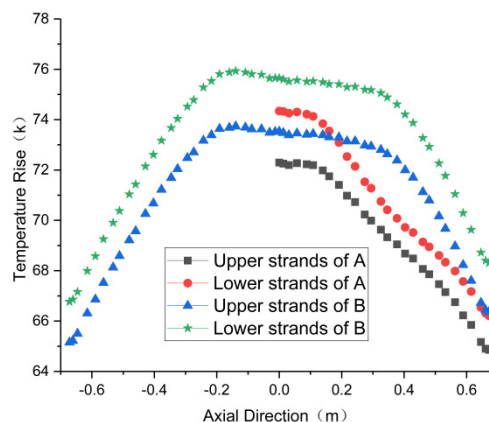**FIGURE 10.** Temperature rise distribution of section z = 0.5185m.

of scheme B is 76.87k. Overall, the average temperature rise of Scheme B is slightly higher than that of Scheme A. The temperature rise in stator region is higher, and the highest temperature rise occurs in lower strands. The cooling effect at the core of the rotor is the best, owing to the strong heat exchange ability between the rotor and the axial cooling ducts of the rotor. As the cooling medium flows through the radial cooling ducts of the rotor and air gap then enters the radial cooling ducts of the stator, that is the upper strand is cooled first, so the temperature rise of the lower strand is slightly higher than that of the upper strand. As it can be further observed in two tables, the temperature rise in the rotor region of scheme B is lower than that of scheme A, while the temperature rise of other parts is higher.

In order to study the temperature rise distribution of each component in the generator in detail, the radial section z = 0.5185m in the solution region is used for the numerical calculation of temperature field. The temperature rise distribution is shown in Fig. 10.

The comparison shows that the radial temperature rise distribution of the two schemes is basically similar, which is consistent with the data in TABLE 3 and 4. The temperature distribution first increases and then decreases. At y = 0.6m,

namely, in the stator region, the temperature increases sharply and the highest temperature is in the stator strand. The temperature drops sharply at about y = 0.75m, which is due to the enlargement of the active area of the cooling medium and the convection of heat transfer with the ventilation duct of the external air path, thus enhancing the heat dissipation effect. As the fluid and ventilation duct heat exchange many times, the heat dissipation effect is improved, and the temperature of the two schemes is getting closer and closer. The curve fluctuates at y = 1m and the amplitude becomes smaller and smaller. Moreover, the temperature near the winding is obviously higher than that in other areas, because the stator winding is the main heat source of the generator, and most of the heat is generated by the windings.

It can be seen from the above analysis that temperature rise in the stator is higher in both regions. Therefore, this paper further analyses the temperature rise distribution law of stator strand. The distribution of axial temperature rise is shown in Fig. 11.

FIGURE 11. Axial temperature rise distribution of stator strands.

From Fig. 11, we can see that in the axial direction, the first half of scheme B gradually increases, while the distribution of the second half tends to be consistent with scheme A, showing a downtrend. The maximum temperature rise of scheme A is 74.46k, which is 1.49k lower than that of scheme B. The temperature rise of upper layer is lower than that of lower layer, and the maximum temperature rise of the upper and lower layers of the two schemes differs by 2.04k and 2.23k respectively. Air enters the cooling stator region from the air gap, and then the temperature rises after heat absorption, so the cooling capacity of both axial and radial direction decreases.

VI. CONCLUSION
1) It is very important to choose a suitable solution region model because the setting will affect the numerical results of electric machine.

2) The generator studied in this paper sets half of the axial section as the solution region, and the error is within the allowable range, but compared with the whole axial segment,

the fluid in the generator is not fully developed, which affects the temperature rise distribution.

3) The temperature rise of stator strand is the highest under rated conditions, while that of rotor core and rotor magnetic steel is relatively low. The vortex flow in the stator tail and air cavity causes uneven heat dissipation inside the generator.

REFERENCES

[1] B. Zhang, R. Qu, J. Wang, W. Xu, X. Fan, and Y. Chen, "Thermal model of totally enclosed water-cooled permanent-magnet synchronous machines for electric vehicle application," *IEEE Trans. Ind. Appl.*, vol. 51, no. 4, pp. 3020–3029, Jul. 2015.

[2] J. Dong, Y. Huang, L. Jin, H. Lin, and H. Yang, "Thermal optimization of a high-speed permanent magnet motor," *IEEE Trans. Magn.*, vol. 50, no. 2, pp. 749–752, Feb. 2014.

[3] S. Ding, G. Cui, Z. Li, and T. Guan, "Fluid and thermal performance analysis of PMSM used for driving," *Heat Mass Transf.*, vol. 52, no. 3, pp. 571–579, 2016.

[4] X. Fan, R. Qu, J. Li, D. Li, B. Zhang, and C. Wang, "Ventilation and thermal improvement of radial forced air-cooled FSCW permanent magnet synchronous wind generators," *IEEE Trans. Ind. Appl.*, vol. 53, no. 4, pp. 3447–3456, Jul./Aug. 2017.

[5] X. H. Qian, Y. L. Jiang, and D. F. Cheng, "Structural design and improvement of wind-driven generator cooling system," *Adv. Mater. Res.*, vols. 1025–1026, pp. 128–136, Sep. 2014.

[6] M. Polikarpova, P. Ponomarev, P. Röyttä, S. Semken, Y. Alexandrova, and J. Pyrhönen, "Direct liquid cooling for an outer-rotor direct-drive permanent-magnet synchronous generator for wind farm applications," *IET Electr. Power Appl.*, vol. 9, no. 8, pp. 523–532, 2015.

[7] D. H. Lim and S. C. Kim, "Thermal performance of oil spray cooling system for in-wheel motor in electric vehicles," *Appl. Thermal Eng.*, vol. 63, no. 2, pp. 577–587, 2014.

[8] Y. Alexandrova, R. S. Semken, and J. Pyrhönen, "Permanent magnet synchronous generator design solution for large direct-drive wind turbines: Thermal behavior of the LC DD-PMSG," *Appl. Therm. Eng.*, vol. 65, nos. 1–2, pp. 554–563, 2014.

[9] R. Camilleri, D. A. Howey, and M. D. McCulloch, "Predicting the temperature and flow distribution in a direct oil-cooled electrical machine with segmented stator," *IEEE Trans. Ind. Electron.*, vol. 63, no. 1, pp. 82–91, Jan. 2016.

[10] M. Polikarpova, P. Lindh, C. Gerada, M. Rilla, V. Naumanen, and J. Pyrhönen, "Thermal effects of stator potting in an axial-flux permanent magnet synchronous generator," *Appl. Therm. Eng.*, vol. 75, pp. 421–429, Jan. 2015.

[11] Y. Liu, C. Li, G. Fu, S. Gao, Y. Tian, and Y. Zhai, "Study of three-dimensional temperature field with changed structures of air-cooled turbo generator stator," *Int. J. Control Autom.*, vol. 8, no. 5, pp. 37–42, 2015.

[12] J. Pyrhönen, P. Lindh, M. Polikarpova, E. Kurvinen, and V. Naumanen, "Heat-transfer improvements in an axial-flux permanent-magnet synchronous machine," *Appl. Therm. Eng.*, vol. 76, pp. 245–251, Feb. 2015.

[13] S. Jia, R. Qu, J. Li, X. Fan, and M. Zhang, "Study of direct-drive permanent-magnet synchronous generators with solid rotor back iron and different windings," *IEEE Trans. Ind. Appl.*, vol. 52, no. 2, pp. 1369–1379, Mar./Apr. 2015.

[14] J. Han, W. Li, L. Wang, X. Zhou, X. Zhang, and Y. Li, "Calculation and analysis of the surface heat-transfer coefficient and temperature fields on the three-dimensional complex end windings of a large turbogenerator," *IEEE Trans. Ind. Electron.*, vol. 61, no. 10, pp. 5222–5231, Oct. 2014.

[15] C. Jungreuthmayer, T. Bauml, O. Winter, M. Ganchev, H. Kapeller, A. Haumer, and C. Kral, "A detailed heat and fluid flow analysis of an internal permanent magnet synchronous machine by means of computational fluid dynamics," *IEEE Trans. Ind. Electron.*, vol. 59, no. 12, pp. 4568–4578, Dec. 2012.

[16] Y. Xu, Y. Jia, M. Ai, and Y. Wang, "Heat transfer characteristics of external ventilated path in compact high-voltage motor," *Int. J. Heat Mass Transf.*, vol. 124, pp. 1136–1146, Sep. 2018.

[17] X. Zhao, Y. Fan, W. Li, D. Li, J. Cao, and Y. Zhang, "Optimization of ventilation spacer for direct-drive permanent magnet wind generator," *Energies*, vol. 12, no. 7, p. 1430, 2019.

[18] Y. Liang, H. Yu, and X. Bian, "Finite-element calculation of 3-D transient electromagnetic field in end region and eddy-current loss decrease in stator end clamping plate of large hydrogenerator," *IEEE Trans. Ind. Electron.*, vol. 62, no. 12, pp. 7331–7338, Oct. 2015.

[19] H. Jichao, G. Baojun, T. Dajun, Z. Hongsen, X. Fang, and W. Li, "Calculation and analysis of complex fluid flow and thermal fields in a fully air-cooled hydrogenerator," *Int. J. Therm. Sci.*, vol. 116, pp. 278–286, Jun. 2017.

[20] S. Ding, F. Meng, and Y. Ge, "Temperature field investigation of canned primary pump motors in nuclear power stations," *Proc. CSEE*, vol. 32, no. 36, pp. 149–155, 2012.

[21] H. J. Feng, S. Y. Ding, and P. Zhou, "Calculation of 3D whole domain steady temperature fields for TEFC motor," *Electr. Mach. Control*, vol. 21, no. 7, pp. 87–93, 2017.

SHUYE DING was born in 1978. He received the B.S., M.S., and Ph.D. degrees from the Harbin University of Science and Technology, Harbin, in 2001, 2004, and 2008, respectively, all in electrical machinery and appliance.

He is currently a Professor with the School of Electrical and Automation Engineering, Nanjing Normal University, Nanjing, China. He is the author or coauthor of more than 80 published peer-reviewed papers and holds more than 10 patents. His research interests include synthesis physical fields of large electrical machines and theoretical study of special electrical machines.

MIN ZHU was born in Yancheng, China, in 1995. She received the B.S. degree in electronic engineering and automation from Nanjing Normal University, in 2017.

Her research direction is the numerical calculation and analysis of temperature and fluid field in the electrical machine.

YING WANG was born in Lianyungang, China, in 1996. She received the B.S. degree in electronic engineering and automation from the Chengxian College, Southeast University, in 2018.

She mainly studies the temperature field and fluid field of motors.

WEI LIU was born in Yancheng, China, in 1997. She is currently pursuing the M.S. degree with Nanjing Normal University, Nanjing, China.

Her research direction is the numerical calculation and analysis of temperature and fluid field in the motors.

● ● ●